EWOD-aided droplet transport on texture ratchets

Cite as: Appl. Phys. Lett. 116, 093702 (2020); https://doi.org/10.1063/1.5142571 Submitted: 14 December 2019 . Accepted: 15 February 2020 . Published Online: 02 March 2020

Di Sun 🗓, and Karl F. Böhringer 🗓







ARTICLES YOU MAY BE INTERESTED IN

Increased droplet coalescence using electrowetting on dielectric (EWOD) Applied Physics Letters 116, 073702 (2020); https://doi.org/10.1063/1.5140202

Fundamental limits of jumping droplet heat transfer Applied Physics Letters 116, 093701 (2020); https://doi.org/10.1063/1.5141744

Cassie-Wenzel wetting transition on nanostructured superhydrophobic surfaces induced by surface acoustic waves

Applied Physics Letters 116, 093704 (2020); https://doi.org/10.1063/1.5145282





EWOD-aided droplet transport on texture ratchets

Cite as: Appl. Phys. Lett. 116, 093702 (2020); doi: 10.1063/1.5142571 Submitted: 14 December 2019 · Accepted: 15 February 2020 · Published Online: 2 March 2020







Di Sun 🕞 and Karl F. Böhringer 🗈 🕞



AFFILIATIONS

Department of Electrical and Computer Engineering and Institute for Nano-Engineered Systems (NanoES), University of Washington, Seattle, Washington 98195, USA

a) Electronic mail: karlb@uw.edu. Tel.: +1-206-221-5177

ABSTRACT

We report a digital microfluidic device to transport aqueous droplets on an open surface in air using electrowetting-on-dielectric (EWOD) with anisotropic ratchet conveyors (ARCs). ARCs are micro-sized periodic semicircular hydrophilic regions on a hydrophobic background, providing anisotropic wettability. SiN_x and Cytop are used as the dielectric layer between the water droplet and working electrodes. By adopting parylene as a stencil mask, hydrophilic patterning on the hydrophobic Cytop thin film layer is achieved without the loss of Cytop hydrophobicity. While the traditional EWOD platform requires the control of multiple electrodes to transport the droplet, our system utilizes only two controlling electrodes. We demonstrate that 15 µl water droplets are transported at a speed of 13 mm/s under 60 V_{peak} sinusoid AC signal at 50 Hz. Droplet transport at 20 Hz is also presented, demonstrating that the system can operate within a range of frequencies.

Published under license by AIP Publishing. https://doi.org/10.1063/1.5142571

Electrowetting, which alters surface energy with an externally applied electric field, is widely used to manipulate fluids at the micro/ nano-scale. Electrowetting-on-dielectric (EWOD) involves a configuration where an insulating dielectric layer and a hydrophobic layer are deposited on top of the working electrodes, separating the electrodes from the working fluid above^{1,2} to reduce electrochemical hydrolysis reactions. The EWOD technique enables many digital fluidic applications such as lab-on-a-chip microfluidic platforms, 3,4 video-speed displays,⁵ focusing lenses,⁶ water collection,⁷ and self-cleaning surfaces.⁸ Many EWOD designs require applying DC voltage sequentially on a series of electrodes. An array of electrodes and dedicated control and addressing circuitry are both necessary to transport the droplet across the substrate.

To simplify the design and wiring complexity, several different types of "continuous electrowetting" prototypes have been explored, in which the droplet can be continuously transported. Lee and Kim applied voltage to an enclosed electrolyte channel containing liquid metal drops. Due to the resistive effect of the electrolyte channel, a voltage difference arose between the two ends of the liquid metal slug. The electrical double layer (EDL) at the metal-electrolyte interface was modulated to create an imbalance in surface tension that propelled the droplet to the lower voltage side. Nelson et al. 10 and Ni et al. 11 developed continuous rectified electrowetting by combining diode-like structures patterned on a stripe of a highly resistive electrode. Due to the resistive voltage gradient, as the water droplet was applied to the electrode surface, the diodes underneath the water droplet were either forward biased or reverse biased. The charge built up solely on the reversely biased diode side causing a surface energy change. The droplet thus moved continuously toward the more positive voltage side. By incorporating an AC square wave signal at mediate frequencies (1 kHz) with a different DC bias, micro-stepping of the droplet could also be implemented on diode-like coplanar electrodes covered by leaky dielectric layers. 12

In our paper, different from the DC EWOD and continuous EWOD methods mentioned above, we use an AC EWOD actuation approach combined with surface micropatterning to transport the droplet with a reduced number of electrodes. AC EWOD has been used to create global droplet shape oscillations by local capillary force alternations near the contact line in the capillary regime. ¹³ In order to transport the droplet, periodic hydrophobic/hydrophilic micro-sized patterns, termed as anisotropic ratchet conveyors (ARCs), also known as texture ratchets, are required to provide anisotropic hysteresis force during each droplet shape oscillation cycle. This approach builds on prior results with mechanical systems, 14,15 where orthogonal vibrations have been applied globally on the whole substrate to create periodic expansion and contraction of the droplet. By combining AC EWOD and ARC, we can reduce the complexity of the addressing circuitry design and control the movement using only two globally controlled electrodes.

We first characterize the static response of droplet contact angle change with an external DC voltage. Figure 1(a) shows the experimental testbench setup in the insets. The experimental contact angle measurements and theoretical calculations of the water droplet contact

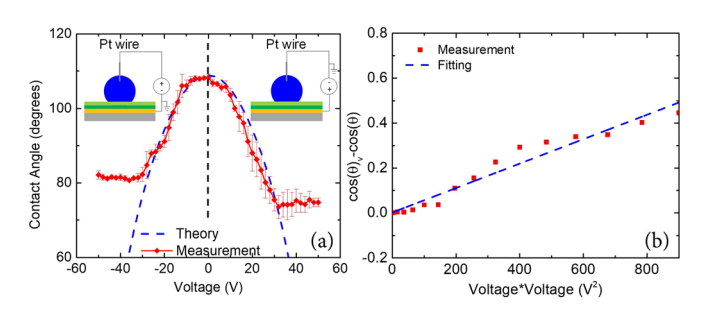


FIG. 1. (a) Experimental results of the static contact angle change under an applied DC electrical field for a sessile water droplet on a Cytop coated substrate without ARC patterns. The contact angle eventually saturates without further decreasing with increased voltage magnitude. (b) The linear fit plot of the experimental results for $(\cos(\theta_V) - \cos(\theta))$ vs V^2 .

angle change under the applied voltage are shown together. A 10 μ l water droplet was applied on top of a gold electrode, with SiN_x and Cytop as the dielectric layer. A platinum probe (30 gauge) electrode was inserted on top of the water droplet. Two voltage-polarity configurations were tested, shown in the insets of Fig. 1(a).

According to the Young–Lippman equation, the apparent water droplet contact angle is determined by the following equation under the external DC voltage:

$$\cos(\theta_V) = \frac{\gamma_{SG} - \gamma_{SL(V)}}{\gamma_{LG}} = \frac{\gamma_{SG} - \gamma_{SL}}{\gamma_{LG}} + \frac{CV^2}{2\gamma_{LG}} = \cos(\theta) + \frac{CV^2}{2\gamma_{LG}}, \quad (1)$$

where γ_{SG} , γ_{SL} , and γ_{LG} are surface tensions at the solid–gas, solid–liquid, and liquid–gas interfaces, respectively. $\gamma_{SL(V)}$ is the solid–liquid surface tension under external electrical voltage. θ_V is the apparent contact angle under the applied voltage. C is the equivalent capacitance between the water droplet and the electrode, with Cytop and SiN $_x$ as the dielectric layers. In the experimental setup, the film thicknesses and dielectric constants for SiN $_x$ and Cytop were $d_{\text{SiNx}}=220\,\text{nm}$, $\varepsilon_{\text{SiNx}}=4.2$ and $d_{\text{Cytop}}=100\,\text{nm}$, $\varepsilon_{\text{Cytop}}=2.1$, respectively, and $\varepsilon_0=8.85\times 10^{-12}\,\frac{\text{F}}{\text{m}}$ is the vacuum permittivity. The equivalent capacitance C can be determined by

$$\frac{1}{C} = \frac{1}{C_{\text{SiN}x}} + \frac{1}{C_{Cytop}} = \frac{C_{\text{SiN}x} + C_{Cytop}}{C_{\text{SiN}x}C_{Cytop}},$$
(2)

resulting in $C=\left(\frac{\epsilon_0}{d_{\rm SiNx}/\epsilon_{\rm SiNx}+d_{\rm Cystep}/\epsilon_{\rm Cystep}}\right) \approx 8.85 imes 10^{-5} \, {
m F/m^2}.$ The mea-

surement results corresponded well with the theoretical calculation. Figure 1(b) shows a linear relation between $\cos(\theta_v) - \cos(\theta)$ and V^2 below the saturation voltage of approximately ± 35 V DC, beyond which the droplet contact angle stopped decreasing with a further increase in the voltage magnitude. The total capacitance of the electrowetting experimental setup can be derived from the slope of the fitting line by solving Eq. (1) for C_2 , which was on the order of 8.2×10^{-5} F/m².

We then designed our AC EWOD system, as shown in Fig. 2, with coplanar electrodes, which consisted of one center electrode and two side electrodes. The side electrodes were connected at one single end. AC voltage was applied between the center and side electrodes to sustain a global droplet shape oscillation by the periodic alternating EWOD force. In terms of surface patterning process, direct patterning on hydrophobic thin films (e.g., Teflon, Cytop) is difficult to

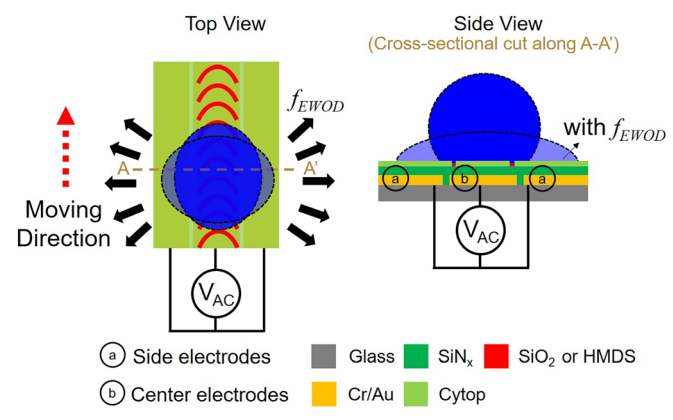


FIG. 2. The top view and side view schematic of the coplanar EWOD system with ARC texture patterns. The dashed line between A and A' from the top view plot on the left represents the cross-sectional cut plane for the side view plot on the right. The water droplet oscillates due to the EWOD force (f_{EWOD}) when an AC signal is applied, which is demonstrated by the partial overlapping of the spherical droplet and the flattened droplet by f_{EWOD} on the hydrophobic Cytop surface. The semi-circular ARC rungs provide an anisotropic wetting force on the leading and trailing edge of the droplet, causing the directional movement of the droplet.

accomplish using standard photolithography. Methods have been proposed to reduce the surface hydrophobicity like plasma treatment or adhesion layer but the original surface properties will be altered, resulting in water droplet contact angle decrease after surface treatment. To solve this problem, we adopted parylene-C as a stencil mask and created hydrophilic patterns on top of the Cytop surface without degrading the original surface properties.

The system was fabricated on a 4" soda-lime glass wafer. 10 nm Cr and 50 nm Au were patterned by electron beam evaporation to create coplanar electrodes using a lift-off process. The SiNx layer was deposited using PECVD. Diluted Cytop (Cytop: CT-Solv 180 = 1:3) was spin-coated and cured at 200 °C for 1 h. The wafer was coated with 2.5 μ m parylene-C as the stencil mask. 10 nm Al was evaporated on the parylene-C surface as an etch stop mask and patterned to define the ARC tracks. The exposed parylene-C area was etched with RIE. The wafer was coated with 50 nm SiO₂ by electron beam evaporation or treated with hexamethyldisilazane (HMDS) by spin coating. The parylene-C layer was carefully peeled off using tweezers before further testing. AC signals were provided by a function generator and amplified by a voltage amplifier (PZD700, Trek Co.) with a voltage amplifying factor of 200 V/V. A water droplet with 15 μ l volume was pipetted and the droplet silhouette monitored by a high-speed camera (FASTCAM Mini UX100) with a sampling rate of 2000 fps.

When applying an AC voltage on the coplanar electrodes, the water droplet started to oscillate laterally driven by the alternating electrowetting force. Simultaneously, the portion of the solid-liquid-air three-phase contact line (TPL) on the center electrode recessed and advanced in response to the droplet expanding and contracting laterally. We denoted the contact line aligned with the ARC semicircular pattern as the leading edge and the opposite side as the trailing edge. Like in prior experiments where the droplets were driven by orthogonal vibration, ¹⁴ both leading and trailing edges periodically wetted and dewetted the ratchets at hydrophobic/hydrophilic boundaries of the ARC pattern. Due to the periodic semicircular shape of the ARC

design, anisotropic hysteresis force occurred at the TPL causing the droplet to move toward the direction of the ARC curve.

The top view of the system with its dimensions after fabrication is shown in Fig. 3(a) and a detailed picture of the ARC pattern with its dimensions is shown in Fig. 3(b). The ARC rungs are designed to match approximately the curvature of the footprint of the droplet. 14,15 A typical movement of the water droplet's leading and trailing edges with time is plotted in Fig. 3(c). The leading and trailing edges expanded at $0.23 \pm 0.019 \,\mathrm{mm}$ and $0.21 \pm 0.013 \,\mathrm{mm}$, respectively, from the initial position in the expansion phase, while the leading and trailing edge recessed $0.11 \pm 0.015 \,\mathrm{mm}$ and $0.33 \pm 0.007 \,\mathrm{mm}$ in the contraction phase. The leading edge conformed to the hydrophilic ARC rungs, creating a longer TPL and thus a higher pinning force than the trailing edge, which made only intermittent contact with the hydrophilic rungs. The anisotropic hysteresis force caused the water droplet to move forward. When an alternating electrical field $(V(t) = V_0 \sin \omega t)$ was applied, the EWOD force could be described as $f_{\text{EWOD}} = \frac{1}{2}CV^2$ (measured in N/m), which is proportional to $(1 - \cos 2\omega t)V_0^2$, driving the droplet to oscillate at twice the frequency of the AC voltage.¹⁹ The droplet oscillation frequency in our case was equal to 100 Hz, corresponding to 50 Hz AC voltage applied. The average droplet movement speed can be estimated by checking either the leading or the trailing edge position change over a certain period. As shown in Fig. 3(c), the total position change of the trailing edge (ΔY) is approximately 1.3 mm within 100 ms of transport time, which results in an estimated transport speed of 13 mm/s.

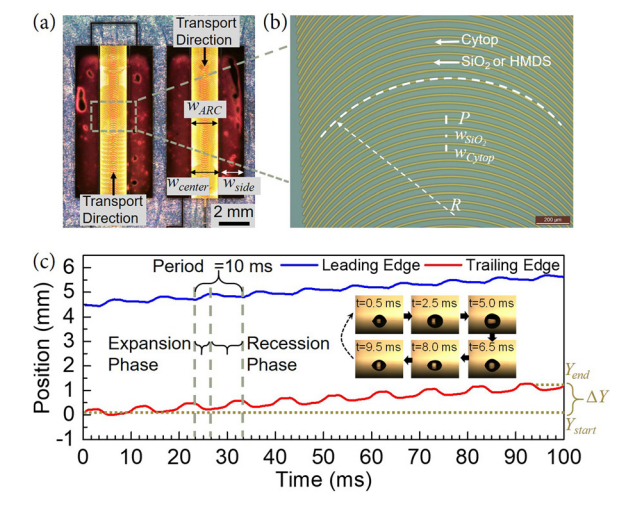


FIG. 3. (a) Top view of the fabricated device. Two ARC tracks with opposite droplet transport directions are shown side by side. The width of the center electrodes (w_{center}) is 2 mm, the side electrode width (w_{side}) is 1.5 mm, and the gap between the electrodes is 50 μ m. The width of the ARC (w_{ARC}) is 1.76 mm. (b) Optical microscope image of the ARC patterns. The rung period pitch (p) is 50 μ m, with the hydrophilic stripe width (w_{SiO_2}) of 10 μ m and the hydrophobic stripe width (w_{Clop}) of 40 μ m. The radius of curvature (r) for the ARC is 1000 μ m. (c) Change in position of leading and trailing edges of a 15 μ l water droplet on the Cytop-SiO₂ surface with time. The applied voltage was a 60 V_{peak} sinusoid signal at 50 Hz. Insets show water droplet silhouettes recorded by the high-speed camera within one period (T=10 ms). The droplet transport speed can be estimated by the trailing edge position change $(\Delta Y=Y_{start}-Y_{end})$ over the measurement period (100 ms).

The droplet motion originates from the force asymmetry and hysteresis at the leading and trailing edges of the contact line on the ARC, which consists of heterogeneous regions with hydrophobic/hydrophilic patterns. The effective force exerted on the contact line along the axis of the ARC can be described as

$$F = d\gamma_{LG}\cos\theta_{app} = d\gamma_{LG}(\chi_{phob}\cos\theta_{phob} + \chi_{phil}\cos\theta_{phil} + \chi_{b}\cos\theta_{b}),$$
(3)

where θ_{app} is the apparent contact angle, d is the diameter of the droplet, γ_{LG} is the liquid–gas surface tension, and θ_{phob} , θ_{phil} , and θ_b are the respective equilibrium contact angles on the hydrophobic material, on the hydrophilic material, and on their boundary, respectively. χ_{phob} , χ_{phil} , and χ_b are the portions of the contact line on the respective materials projected orthogonally to the axis of the ARC. As stated in prior work, this projection effectively extracts the component of the force vector in the direction of the ARC axis and uses the linefraction-modified Cassie-Baxter equation.²⁰ To understand the droplet behavior, we need to look at the force asymmetry between the leading and trailing edges of the droplet as the TPL advances and recedes. The interactions between TPL and ARC rungs exhibit different behaviors for leading and trailing edges, and for advancing and receding regimes. Consequently, we derive separate force expressions for the leading and trailing edge, and for advancing and receding TPL. For these four scenarios, the corresponding effective force in Eq. (3) can be described with $F_{lead,adv}$, $F_{trail,adv}$, $F_{lead,rec}$, and $F_{trail,rec}$, respectively,

$$F_{lead,adv} = d\gamma_{LG} (\chi_{lead,phob} \cos \theta_{phob,adv} + \chi_{lead,phil} \cos \theta_{phil,adv} + \chi_{lead,h} \cos \theta_{b,adv}), \tag{4}$$

$$F_{trail,adv} = d\gamma_{LG} (\chi_{trail,phob} \cos \theta_{phob,adv} + \chi_{trail,phil} \cos \theta_{phil,adv} + \chi_{trail,b} \cos \theta_{b,adv}),$$
(5)

$$F_{lead,rec} = d\gamma_{LG} \left(\chi_{lead,phob} \cos \theta_{phob,rec} + \chi_{lead,phil} \cos \theta_{phil,rec} + \chi_{lead,b} \cos \theta_{b,rec} \right), \tag{6}$$

$$F_{trail,rec} = d\gamma_{LG} \left(\chi_{trail,phob} \cos \theta_{phob,rec} + \chi_{trail,phil} \cos \theta_{phil,rec} + \chi_{trail,b} \cos \theta_{b,rec} \right). \tag{7}$$

Force asymmetry occurs when $F_{asym,adv} = F_{lead,adv} + F_{trail,adv} \neq 0$ or $F_{asym,rec} = F_{lead,rec} + F_{trail,rec} \neq 0$, i.e., when there is a non-zero net force while the contact line advances or recedes. We define the TPL portions such that $\chi_{lead,phob} + \chi_{lead,phil} + \chi_{lead,b} = 1$ for the leading edge and $\chi_{trail,phob} + \chi_{trail,phil} + \chi_{trail,b} = -1$ for the trailing edge to take into account the opposing force directions at the leading and trailing edges. All the absolute χ values are in the range between 0 and 1. Due to the ARC design, the leading edge will pin along a hydrophobic rung while advancing $(\theta_{b,adv} = \theta_{phob,adv})$ and along a hydrophilic rung while receding $(\theta_{b,rec} = \theta_{phil,rec})$. The force anisotropy can be described as

$$F_{an} = F_{asym,adv} + F_{asym,rec}.$$
 (8)

 F_{an} provides an indication on the expected movement of the droplet. For example, a larger positive value of F_{an} suggests a faster movement in the positive direction. Note that $F_{asym,adv}$ and $F_{asym,rec}$ assume pinning of the TPL on the ARC patterns and are therefore peak force values, which occur at different times in the voltage oscillation cycle.

Therefore, F_{an} is useful as a design parameter but does not capture the complete dynamics of the droplet behavior, which would require the integration of the time-varying pinning forces along the TPL over the heterogeneous ARC surface.

To maximize the force anisotropy, $\chi_{trail,phil}$ should be as small as possible and $\chi_{trail,phob}$ should be as large as possible. In addition, the forward force increases with a larger difference between the hydrophilic and hydrophobic contact angles. As noted above, while the TPL moves across the ARC substrate, the χ values may vary with time. To simplify our analysis, we base the following calculations on the maximum forces that the ARC can exert on the droplet, which correspond to the maximum pinning of the TPL along the heterogeneous ARC pattern.

Figure 4(a) shows a typical scenario when the droplet rests on the ARC rungs. The leading edge of the droplet continuously wets along the hydrophilic/hydrophobic boundaries while the trailing edge has intermittent contact with hydrophobic and hydrophilic regions. By inserting the empirically determined χ values from Fig. 4(a) and the contact angle hysteresis data of hydrophobic and hydrophilic materials into Eq. (3), we can calculate the apparent contact angle hysteresis at the leading and trailing edges during advancing and receding. We experimentally measured the advancing and receding angle of Cytop and HMDS using a drop shape analyzer (KRÜSS DSA100L). With $\theta_{phob,adv} = 115^{\circ}$, $\theta_{phob,rec} = 101^{\circ}$, $\theta_{phil,adv} = 79^{\circ}$, and $\theta_{phil,rec} = 64^{\circ}$, we obtain $\cos \theta_{app,lead,adv} = -0.42$, $\cos \theta_{app,trail,adv} = 0.32$, $\cos \theta_{app,lead,rec}$ =0.35, and $\cos \theta_{app,trail,rec}$ = -0.01. Further, with d = 3 mm and $\gamma_{LG} = 0.072 \text{ N/m}$, we get $F_{lead,adv} = -91.3 \mu\text{N}$, $F_{trail,adv} = 75.7 \mu\text{N}$, $F_{lead,rec} = 70.1 \,\mu\text{N}$, and $F_{trail,rec} = -2.3 \,\mu\text{N}$. The force asymmetry during advancing and receding is $F_{asym,adv} = -15.6 \mu N$ and $F_{asym,rec}$ = 67.8 μ N, respectively. From Eq. (8), the results imply force anisotropy of $F_{an} = 52.2 \mu N$ toward the moving direction.

Figure 4(b) plots the corresponding contact angle change of the leading and trailing edges with time. We observed that within each cycle, the leading edge had larger apparent contact angle hysteresis than the trailing edge, leading to larger hysteresis forces over each vibration cycle. Our system can transport a range of droplet sizes within a certain frequency bandwidth under a fixed voltage amplitude

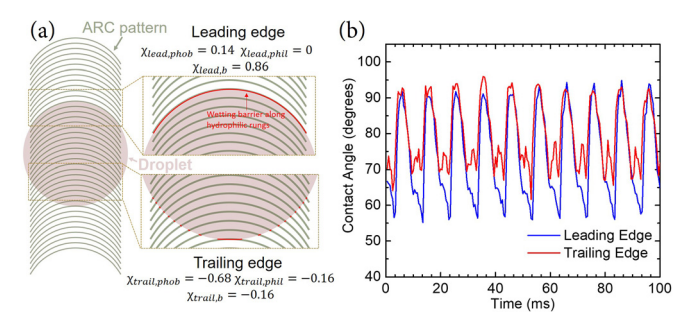


FIG. 4. (a) Schematic of a droplet on an ARC surface. In the drawing, the diameter of the droplet is 3 mm. The radius of the rung is 1.5 mm with a rung width of 10 μ m. We use image processing techniques to obtain an estimated value $\chi_{lead,b}$ for the projected wetting barrier length along the leading edge. For the trailing edge, we assume $\chi_{trail,phil} = \chi_{trail,b}$. (b) The contact angle change of droplet leading and trailing edge with time. Pinning anisotropy of the leading and trailing edge can be clearly seen during each oscillation cycle period ($T=10 \, \mathrm{ms}$) as a difference in the corresponding contact angles.

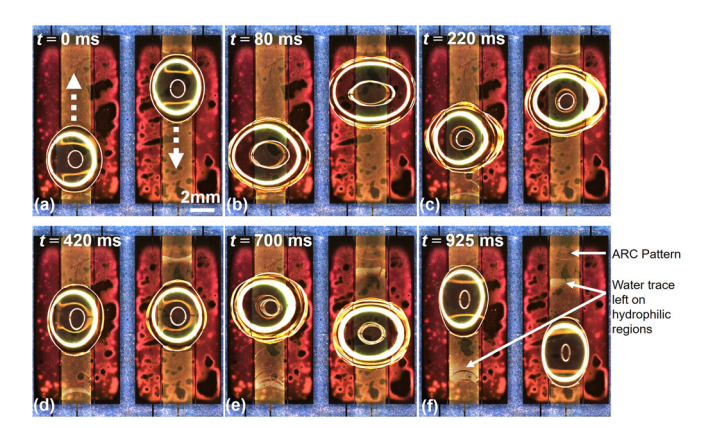


FIG. 5. Top view of water droplet transport under a 20 Hz 60 V_{peak} sinusoid electrical signal on Cytop-SiO $_2$ surface. The two adjacent ARC tracks were designed to transport two droplets in opposite directions at the same time. The droplet transport directions are indicated by the white arrow in (a). We noticed that the water trace on the hydrophilic regions could be reduced by using less hydrophilic surface finish treatment (e.g., hexamethyldisilazane) compared with SiO $_2$.

input. To move a droplet with a volume of 15 μ l, the frequency can vary from 5 to 50 Hz. Figure 5 shows a top view of two ARC ratchets pointing in opposite directions patterned on AC EWOD tracks. Two 15 μ l water droplets were transported with 20 Hz sinusoid AC voltage in the opposite directions simultaneously, demonstrating an EWOD-aided controlled water droplet transportation platform without the need for complex control circuitry.

In conclusion, an EWOD-aided water droplet transport technique was introduced with the help of ARC design. The microscopic patterning technique on a hydrophobic Cytop layer was realized by using parylene as a stencil etching mask. The water droplet static contact angle change was studied and characterized by the specific EWOD system design. Instead of using orthogonal vibrations to the substrate, droplet oscillation was initiated with electrowetting on dielectric. The droplet was transported by the anisotropic force along with the ARC patterns using only two globally controlled electrodes.

See the supplementary material for the experimental process flow diagram, contact angle characterization results of Cytop, and a live demo of droplet transport on the ARC patterned surface.

Fabrication was performed at the Washington Nanofabrication Facility (WNF), a member site of the NSF National Nanotechnology Coordinated Infrastructure (NNCI), with support from NSF Award Nos. ECCS-1308025 and NNCI-1542101. We would like to acknowledge the funding and fellowship support from CoMotion, the Clean Energy Institute at the University of Washington, and the Amazon Catalyst Fund.

REFERENCES

¹W. C. Nelson and C.-J. C. Kim, J. Adhes. Sci. Technol. **26**(12-17), 1747–1771

²H.-W. Lu, F. Bottausci, J. D. Fowler, A. L. Bertozzi, and C. Meinhart, Lab Chip 8(3), 456–461 (2008).

³M. G. Pollack, A. D. Shenderov, and R. B. Fair, Lab Chip 2(2), 96–101 (2002).

- ⁴S. K. Cho, H. Moon, and C.-J. Kim, J. Microelectromech. Syst. 12(1), 70-80
- ⁵R. A. Hayes and B. J. Feenstra, Nature **425**(6956), 383 (2003).
- ⁶S. Kuiper and B. Hendriks, Appl. Phys. Lett. **85**(7), 1128–1130 (2004).
- ⁷R. Yan, T. S. McClure, I. H. Jasim, A. K. R. Koppula, S. Wang, M. Almasri, and C.-L. Chen, Appl. Phys. Lett. 113(20), 204101 (2018).
- ⁸D. Sun and K. F. Böhringer, Micromachines **10**(2), 101 (2019).
- ⁹J. Lee and C.-J. Kim, J. Microelectromech. Syst. **9**(2), 171–180 (2000).
- ¹⁰C. W. Nelson, C. M. Lynch, and N. B. Crane, Lab Chip **11**(13), 2149–2152 (2011).
- ¹¹Q. Ni, D. E. Capecci, M. Schlafly, and N. B. Crane, Microfluid. Nanofluid. **20**(8), 122 (2016).
- ¹²Q. Ni, D. E. Capecci, and N. B. Crane, Sens. Actuators, A **247**, 579–586 (2016).
- ¹³P. Sen and C.-J. C. Kim, Langmuir **25**(8), 4302–4305 (2009).

- ¹⁴T. A. Duncombe, E. Y. Erdem, A. Shastry, R. Baskaran, and K. F. Böhringer, Adv. Mater. 24(12), 1545-1550 (2012).
- 15 T. A. Duncombe, J. F. Parsons, and K. F. Böhringer, Langmuir 28(38), 13765-13770 (2012).
- ¹⁶C.-C. Cho, D. Smith, and J. Anderson, Mater. Chem. Phys. 42(2), 91-95
- ¹⁷S. Makohliso, L. Giovangrandi, D. Leonard, H. Mathieu, M. Ilegems, and P. Aebischer, Biosens. Bioelectron. 13(11), 1227-1235 (1998).
- ¹⁸H. Zhang, Q. Yan, Q. Xu, C. Xiao, and X. Liang, Sci. Rep. 7(1), 3983 (2017).
- ¹⁹E. Baird, P. Young, and K. Mohseni, Microfluid. Nanofluid. 3(6), 635-644 (2007). ²⁰ A. Cassie and S. Baxter, Trans. Faraday Soc. **40**, 546–551 (1944).
- ²¹C. Extrand, Langmuir 19(9), 3793–3796 (2003).